Available online at www.sciencedirect.com
SCIENCE DIRECT
Journal of Sound and Vibration 297 (2006) 267–292
JOURNAL OF SOUND AND VIBRATION
www.elsevier.com/locate/jsvi

Rapid calculation of the compression wave generated by a train entering a tunnel with a vented hood

M.S. Howe[a,*], M. Iida[b], T. Maeda[b], Y. Sakuma[b]

[a]*College of Engineering, Boston University, 110 Cummington Street, Boston MA 02215, USA*
[b]*Railway Technical Research Institute, 2-8-38 Hikari-cho, Kokubunji-shi, Tokyo 185-8540, Japan*

Received 9 May 2005; received in revised form 13 March 2006; accepted 29 March 2006
Available online 14 June 2006

Abstract

A practical analytical scheme is proposed for making rapid numerical predictions of the compression wave generated when a high-speed train enters a tunnel fitted with a vented entrance hood. The method synthesises results from several analytical procedures developed during the past few years for treating different aspects of the tunnel-entry problem, including the effects of change in cross-sectional area at the hood-tunnel junction, high-speed jet flows from windows distributed along the length of the hood, frictional losses associated with separated turbulent flow between the tunnel and hood walls and the train, and the influence of train nose shape. Details are given in this paper for the simplest case of circular cylindrical tunnels and hoods of the type used in model scale testing and design studies. Typical predictions can be made in a few seconds on a personal computer (in contrast to the tens or hundreds of hours required for simulations using the Euler or Navier–Stokes equations on a high performance supercomputer). A summary is given of selected predictions and their comparisons with experiments performed at the Railway Technical Research Institute in Tokyo at train Mach numbers as large as 0.35 (~425 km/h).

1. Introduction

1.1. Background

The pressure rise across the front of the compression wave generated when a train enters a tunnel increases approximately as the square of the train speed U [1–6] and frequently exceeds 2–3% of atmospheric pressure, but the time history and profile of the wave front depend critically on the shape of the train nose and on the geometry of the tunnel portal [7–17]. It is these latter characteristics of the waveform that determine the subjective influence of the wave. When the wave arrives at the distant tunnel exit part of its energy radiates out as a pressure pulse (the *micro-pressure wave*) whose strength is proportional to the compression wave-front steepness. The micro-pressure wave causes 'rattles' and vibrations in buildings near the tunnel exit, particularly when the tunnel is long and equipped with 'acoustically smooth' concrete slab tracks, which tend

*Corresponding author. Tel.: +1 617 484 0656; fax: +1 617 353 5866.
E-mail addresses: mshowe@bu.edu (M.S. Howe), iida@rtri.or.jp (M. Iida).

0022-460X/$ - see front matter © 2006 Elsevier Ltd. All rights reserved.
doi:10.1016/j.jsv.2006.03.039

Nomenclature

A_k	area of kth window
$\mathscr{A}$	cross-sectional area of tunnel
$\mathscr{A}_h$	cross-sectional area of hood
$\mathscr{A}_o$	uniform cross-sectional area of train
$\mathscr{A}_T$	cross-sectional area of train nose
c_o	mean sound speed in tunnel
G	Green's function Eq. (16), (17)
h	uniform radius of model train
$H(x)$	Heaviside unit step function
ℓ_h	length of hood
ℓ_m	distance of microphone from the hood entrance
ℓ_w	thickness of hood wall
ℓ_D	end correction of tunnel and hood combined
ℓ_E	end correction of hood
ℓ_J	hydrodynamic length of junction
ℓ_x	axial length of a window
ℓ_θ	azimuthal length of a window
$\bar{\ell}_k$	variable window end correction, (40)
L	length of nose
L_h	perimeter of train
L_{R_h}	perimeter of hood
L_R	perimeter of tunnel
$\mathscr{L}_k$	length of the jet from kth window
M	train Mach number
p_D	pressure generated by turbulence drag, Section 5
p_{DH}	pressure generated by turbulence drag in hood
p_{DT}	pressure generated by turbulence drag in tunnel
p_E	pressure generated at the hood portal, Section 3.2
p_I	direct pressure incident on a window, (31)
p'_I	see Eq. (32)
p_W	overall pressure generated by the windows, Section 6.3
p'_E	pressure defined in Eq. (9)
p_J	pressure generated at the junction, Section 4.2
p_k	pressure generated at the kth window, Section 6.2
p	compression wave pressure
P_E	entrance pressure, see Section 3.1
P_{JT}	pressure (11) radiated into the tunnel from the junction
P_{JH}	pressure (12) radiated into the hood from the junction
R	tunnel radius
R_h	hood radius
R_k	equivalent radius of kth window
$\mathscr{R}_J$	junction reflection coefficient
$\mathscr{T}_J$	junction transmission coefficient
s	distance measured from nose tip
t	time
$[t]$	retarded time
V_k	mean jet velocity in kth window
v_*	friction velocity
x_k	x-coordinate of the centroid of the kth window
(x, y, z)	coordinate axes
$\mathbf{x}$	(x, y, z)
U	train speed
U_∞	see Eq. (19)
U_{TW}	relative velocity defined in Eq. (20)
U_{HW}	relative velocity defined in Eq. (20)
U_{TT}	relative velocity defined in Eq. (20)
U_{HT}	relative velocity defined in Eq. (20)
z_t	train track offset
$\delta(x)$	Dirac delta function
μ	friction coefficient
ρ_o	mean air density
σ	jet contraction ratio
φ^*_E	potential flow function for hood portal
φ^*_J	potential flow function for the junction
Ψ	pressure transition function defined by Eq. (30)

to promote nonlinear steepening of the front. An uncontrolled, large amplitude micro-pressure wave is heard as a startling 'bang' near the exit portal, very much akin to the sonic-boom that accompanies a supersonic aircraft.

It has long been the practice on the Japanese *Shinkansen* to suppress nonlinear wave steepening by the installation of tunnel entrance hoods [7,8,18,19]. A hood consists of a thin-walled, cylindrical extension ahead of the tunnel, usually with a set of open 'windows' distributed along its length. High pressure air is forced out of the windows by an entering train, as a consequence of which the initial 'rise time' of the compression wave is greatly increased. By judiciously distributing and sizing these windows it has been found possible to produce

up to a 10-fold increase in the wave front thickness and an optimal wave front profile over which the pressure rise is linear.

Hitherto the design of tunnel-entrance hoods has been based almost entirely on data furnished by model scale tests using axisymmetric experimental configurations of the kind depicted schematically in Fig. 1 [7–9,18–23]. The model train is also axisymmetric and is projected into the hood and tunnel at speeds of 400 km/h or more along a tightly stretched wire guide. The influence of hood windows on the compression wave profile is determined from measurements using flush-mounted wall pressure sensors within the tunnel ahead of the train. The Reynolds number is sufficiently large that dissipative processes (including heat transfer) can be neglected during the initial period in which the wave front is formed, so that dynamic similarity with full scale is achieved during the initial stages of wave formation by matching train Mach numbers. Theory [23] and experiments show, however, that flow separation to the rear of the train nose causes an additional slow, but progressive rise in pressure to the rear of the wave front. This component of the wave is associated with a dipole acoustic pressure source produced by the frictional drag experienced by the train in the tunnel and depends on Reynolds number.

There is an obvious advantage to be gained, however, by supplementing model scale testing with a fast and efficient prediction scheme that can be used to identify candidate hood designs. The need for such analytical predictions is made more desirable by the considerable design difficulties posed by the planned introductions of very high speed trains ($U\sim500$ km/h for the advanced *Maglev* train). It is anticipated that such trains will spend 50% or more of a typical journey within a succession of long tunnels, and that hoods 200 m or more in length will be required to suppress nonlinear steepening of the compression wave. In these circumstances a lengthy trial-and-error experimental search for an optimal hood window distribution can be avoided by preliminary numerical analysis.

Vardy and Dayman [24] have developed a fast numerical procedure for calculating pressure transients in tunnels with flared or perforated entrance regions; predictions agree well with measurements provided the values of certain empirical coefficients are carefully chosen. The method is based on the assumption of one-dimensional flow and it cannot, therefore, resolve fine details of the compression wave profile (which depend critically on the multidimensionality of the train, tunnel and flow, associated with the variable geometry of the hood and the hood–tunnel junction, train axis offset, location and size of hood windows, train nose shape, etc) even for an elongated hood. However, such tools have been used to determine basic design specifications such as, for example, blockage and the disposition of air-shafts.

Analytical models that account for the separate contributions to the compression wave profile determined by the shapes and dimensions of the hood, tunnel and train nose, by the high speed jets exhausting from windows arbitrarily distributed in size and position along the sides and roof of the hood, and by the wake formed by turbulent separation just to the rear of the train nose, have been investigated and validated by Howe et al. [20–23,25]. The object of the present paper is to bring together the results of these studies to formulate a compact algorithm for use on a personal computer that is fast enough to permit 'real-time' design studies of the compression wave generated by a train passing through a tunnel entrance hood.

Of course, the compression wave can be predicted by the conventional procedures of computational fluid dynamics (CFD; for example, using the compressible Reynolds averaged Navier–Stokes equations together with a suitable turbulence model, a k–ε model, say) which, moreover, are capable of supplying predictions of the *entire* unsteady flow produced by a train entering a tunnel. The run-times necessary on a high-performance computer for the simplest case of two-dimensional, axisymmetric flow would be several hours. This would be

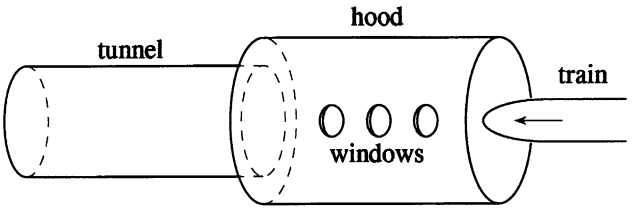

Fig. 1. Schematic illustration of a model scale train entering an axisymmetric cylindrical tunnel and tunnel entrance hood with windows.

increased to several tens or hundreds of hours for a fully three-dimensional problem, involving a train entering a double-tracked tunnel and hood with an asymmetric distribution of windows. Predictions made for the same general case using a prototype of the algorithm proposed in this paper require run times typically of a few seconds on a modern desk-top machine. In addition, the algorithm permits the designer to isolate the different contributions to the compression wave from the interactions of the train nose with: (i) the hood portal, (ii) the junction between the hood and tunnel, (iii) the windows, and (iv) from the separated flow along the sides of the train, and accordingly provides a degree of physical insight into the mechanisms of wave formation that is often difficult to extract from a more complete CFD solution.

1.2. Mechanisms of compression wave generation

The compression wave begins to form just before the train nose enters the hood (see Fig. 2). The train nose is in a first approximation equivalent to a monopole source, whose strength is determined by the rate at which air is displaced by the advancing train, and a dipole directed along the path of the train and equal in magnitude to the drag force on the nose produced by the pressure rise in front of the train. Both of these sources act over the region of the nose where the cross-sectional area $\mathscr{A}_T$ of the train is varying. When the nose approaches and passes the hood entrance plane E of Fig. 2, the interaction of the nose monopole and dipole sources with the portal produces an incipient compression wave p_E, say, that propagates as a plane wave ahead of the train and subsequently interacts with windows W and with the junction J of the hood and tunnel before the arrival of the train [20–22]. At the junction J the wave is partially transmitted into the tunnel and partially reflected back towards the entrance. The interaction of this reflected wave with the train can usually be neglected if the 'blockage' $\mathscr{A}_o/\mathscr{A}_h \leqslant 0.2$, where $\mathscr{A}_o$ is the uniform cross-sectional area of the train to the rear of the nose, and $\mathscr{A}_h$ is the hood cross-section; this is typical of full-scale applications. The reflected wave therefore proceeds to the hood portal E where it is effectively *totally* reflected back towards the tunnel with a reflection coefficient very close to -1; the wave subsequently experiences multiple reflections from the ends of the hood, and each interaction at the junction J results in a fraction of the wave energy being transmitted into the tunnel. In practice no more than about four back-and-forth reflections of p_E are necessary before most of the initial wave energy has passed into the tunnel.

The arrival of the train nose at the junction J results in the generation of a second important pressure wave p_J, which propagates into the tunnel as a compression wave and back towards E as an expansion wave; again, the latter component of this wave experiences multiple reflections from the ends of the hood, but ultimately (after three or four round trips within the hood) most of its energy is transmitted into the tunnel and contributes to an extended profile of the compression wave front.

Consider the simplest case of a hood with *one* window (W in Fig. 2). When the component p_E of the pressure generated at the hood portal first arrives at the window the pressure at the wave front falls rapidly because an open window initially behaves as a pressure node (an 'irrotational volume sink') that generates a pressure fluctuation p_W in the form of an expansion wave. However, vorticity production at the window quickly leads to the formation of a high speed jet whose velocity increases typically to about 50% of the train speed. Jet vorticity behaves as an aeroacoustic source, producing a pressure pulse that arrests the fall in pressure at the window, and causes the compression wave generated at the hood entrance to be transmitted past the window

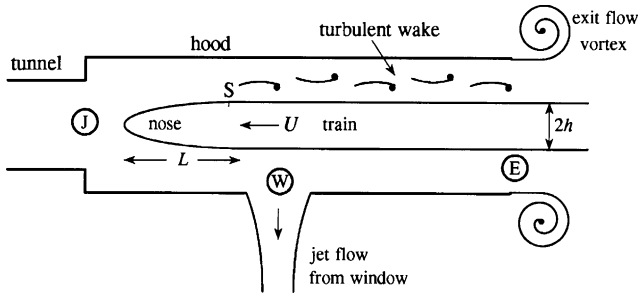

Fig. 2. Illustrating the principal contributing sources to compression wave formation.

at reduced but constant amplitude. Subsequent reflections of this wave from the ends of the hood, and the additional pressure variations at W produced by the wave p_J generated at the junction J cause small fluctuations in jet velocity, but the most significant change in jet velocity occurs when the train nose passes the window [22,25]. The excess pressure at the window decreases rapidly as the nose passes, to a level only marginally higher than atmospheric [25], and the radiation from the window into the tunnel decreases. In the meantime, once the nose has passed the window the pressure in front of the nose rises to a level comparable to the value it would have had if the window had been absent, causing the pressure at the rear of the compression wave front to rise. A similar but obviously more complicated set of interactions occur in the presence of several windows, when in addition waves are reflected at the windows and the separate window jets are coupled by pressures reflected back-and-forth within the hood; these in turn produce further modifications of the compression wave front.

The superposed pressures p_E, p_J, p_W, appropriately modified by reflections from the ends of the hood, dominate the shape of the compression wave front. However, a smaller, additional component p_D is responsible for a gradual and practically linear increase in pressure with distance to the rear of the main pressure rise. This pressure is produced by turbulence in the mean flow between the tunnel walls and the train to the rear of the point labelled S in Fig. 2, near which the flow over the train in the tunnel separates [23]. The turbulent wall flow is produced by the displacement of air by the train nose; a large 'exit flow vortex' is formed (Fig. 2) when this flow emerges from the hood portal [23,26–28]. Calculation and experiment [23] indicate that the vortex makes a relatively small contribution to p_D, but the contribution from the turbulence within the tunnel increases linearly with the distance travelled by the train nose into the tunnel (reaching a peak just before the tail of the train enters the hood) and cannot be neglected. The contribution from the turbulence can be represented by a dipole acoustic source distributed along the surfaces of the train and the tunnel wall between the nose and the hood portal; the overall strength of this dipole is just equal to the drag exerted by the flow on the train and wall, and is clearly proportional to the length of train within the tunnel and hood.

1.3. Contribution of this paper

In this paper analytical representations of the pressures p_E, p_J, p_W, p_D, developed in [20–23,25] are combined to form the basis of a fast numerical algorithm for predicting the initial form of the compression wave. The algorithm is based on *linear acoustics*, so that predictions are valid for a short time during and after the train nose passes through the hood, before nonlinear steepening becomes important. If necessary the subsequent nonlinear evolution of the one-dimensional wave front can be determined by the usual method of characteristics.

The mathematical problem is formulated in Section 2. In Sections 3–6 the formulae for, respectively, the components p_E, p_J, p_D and p_W of the compression wave are reviewed. These are combined in Section 7, where a comparison is made of predictions with model scale test results for train speeds up to 360 km/h for both unvented and vented hoods. Further comparisons are made in Section 8 for hoods with multiple facing windows; Section 9 contains a comparison of predictions with results from more recent tests performed at train speeds ~425 km/h.

2. Formulation

The procedure for calculating the compression wave will be formulated in terms of the configuration depicted in Fig. 3, involving a circular cylindrical tunnel of interior radius R fitted axisymmetrically with a thin-walled, circular cylindrical hood of interior radius R_h and length ℓ_h. This arrangement is typical of that used in model-scale experiments. In particular the hood portal is assumed to be *unflanged*, which corresponds to usual practice at full scale. Take the origin of the coordinates (x, y, z) at the centre O of the hood entrance plane, with the negative x-axis along the common axis of symmetry of the tunnel and hood. For the purpose of calculating the compression wave prior to the onset of nonlinearity and reflections from the distant tunnel exit, it may be assumed that the tunnel extends to $x = -\infty$. Details will be presented for the case in which N windows are distributed in a single row along the wall of the hood, with the centroid of the kth window at $(x_k, 0, R)$, $-\ell_h < x_k < 0$ (i.e. along the line of intersection of the xz-plane in $z > 0$ with the hood); the figure

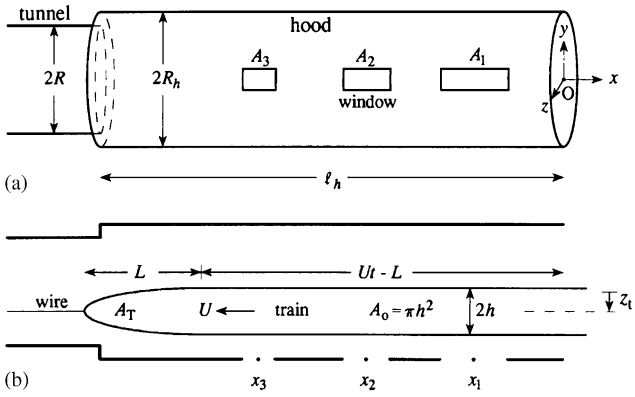

Fig. 3. Parameters defining the configuration of the hood, tunnel and axisymmetric train: (a) 'side' view from the direction of the positive z-axis; (b) 'top' view from the direction of the positive y-axis.

illustrates this for $N = 3$. Let A_k denote the area of the kth window. In general it will be assumed that $A_k \ll \mathscr{A}_h = \pi R_h^2 \equiv$ cross-sectional area of the hood. It will be seen (in conformity with previous studies [22,25]) that predictions are to a good approximation independent of the window *shape*, and the method to be used (in Section 6) to analyse the interaction of the train nose with a window is formally based on the hypothesis that the window is *circular*. Long, slit-like windows can be approximated by a linear sequence of small circular windows; examples of this are discussed in Sections 7 and 8. The thickness ℓ_w of the hood wall at the window *is* important (since it makes a significant contribution to the effective acoustic *admittance* of the window). It is assumed that ℓ_w takes the same constant value for all windows, although this can obviously be changed to suit particular circumstances.

In the usual experimental arrangement an axisymmetric model train is guided along the tunnel by a tightly stretched wire that passes smoothly through a cylindrical channel bored along the train axis. The 'top' view in Fig. 3b shows the wire displaced a distance $z_t > 0$ from the tunnel axis *towards the windows* (in the z-direction). The two cases $z_t \gtrless 0$ therefore correspond, respectively, to a train travelling along a track adjacent to the windows or far from the windows. The train has circular cylindrical cross-section of radius h and area $\mathscr{A}_o = \pi h^2$ except within a distance L from the tip of the train nose, where the area $\mathscr{A}_T(s)$, say, varies in a prescribed manner with distance s measured from the nose tip. The train is projected along the wire into the tunnel at uniform speed U, such that nose first cuts the hood entrance plane $x = 0$ at time $t = 0$. After time t the nose and a length $Ut - L$ of the cylindrical section of the train are within the tunnel and hood. The tail section of the experimental train is usually profiled, but this can be ignored, and the uniform part of the train regarded as infinitely long for the purpose of calculating the initial form of the compression wave.

3. Pressure wave generated at the hood portal and its interaction with the junction

3.1. The entrance pressure P_E

The front of the train crosses the entrance plane $x = 0$ of the hood at time $t = 0$. Let c_o denote the speed of sound, and let $P_E(t + x/c_o)$ be the pressure wave ahead of the train produced by the interaction of the train nose with the hood portal when the presence of hood windows is ignored, and for times $t < \ell_h/c_o$ (before reflection at the junction J between the hood and tunnel). This initial interaction of the train with the hood can be regarded as irrotational, occurring before additional pressure sources associated with viscous drag and vorticity production become significant.

For a circular cylindrical hood [21]

$$P_E\left(t + \frac{x}{c_o}\right) \approx \frac{\rho_o U^2}{\mathscr{A}_h(1 - M^2)}\left(1 + \frac{\mathscr{A}_o}{\mathscr{A}}\right)\int_{-\infty}^{\infty} \frac{\partial \varphi_E^*}{\partial x'}(x', 0, z_t)\frac{\partial \mathscr{A}_T}{\partial x'}(x' + U[t])\,\mathrm{d}x', \tag{1}$$

where $M = U/c_o$ is the train Mach number and $\varphi_E^*(\mathbf{x})$ is the solution of Laplace's equation that represents the velocity potential of a hypothetical, uniform incompressible flow *out* of the hood portal satisfying

$$\left.\begin{array}{rcll} \varphi_E^*(\mathbf{x}) & \approx & x-\ell_E & \text{for } |x|\gg R_h \text{ inside the hood} \\ & \approx & -\mathscr{A}_h/4\pi|\mathbf{x}| & \text{for } |\mathbf{x}|\gg R_h \text{ outside the hood} \end{array}\right\}. \tag{2}$$

The length $\ell_E \approx 0.61R_h$ is the Rayleigh *end-correction* [29–31] of a circular cylinder of radius R_h, and

$$[t] = t + \frac{x-\ell_E}{c_o} \tag{3}$$

is the effective retarded time. When the train nose has passed into the hood, Eq. (2) shows that $\partial\varphi_E^*/\partial x' = 1$ in the region where the integrand of Eq. (1) is non-zero, and therefore that the overall initial pressure rise is

$$\frac{\rho_o U^2}{(1-M^2)}\frac{\mathscr{A}_o}{\mathscr{A}_h}\left(1+\frac{\mathscr{A}_o}{\mathscr{A}}\right). \tag{4}$$

The harmonic function $\varphi_E^*(\mathbf{x})$ is calculated for uniform flow from an infinite cylinder of radius R_h *with no windows*, for which

$$\begin{aligned} \frac{\partial\varphi_E^*}{\partial x}(\mathbf{x}) &= \frac{1}{2} - \frac{1}{2\pi}\int_0^\infty I_0\left(\lambda\frac{r}{R_h}\right)\sqrt{\frac{2K_1(\lambda)}{I_1(\lambda)}}\sin\left(\lambda\left[\frac{x}{R_h}+\mathscr{F}(\lambda)\right]\right)\mathrm{d}\lambda, \quad r<R_h, \\ \mathscr{F}(\lambda) &= \frac{1}{\pi}\int_0^\infty \frac{\ln[K_1(\mu)I_1(\mu)/K_1(\lambda)I_1(\lambda)]}{\mu^2-\lambda^2}\,\mathrm{d}\mu, \end{aligned} \tag{5}$$

where $I_0,\ I_1,\ K_1$ are modified Bessel functions and $r = \sqrt{y^2+z^2}$.

3.2. The pressure $p_E(x,t)$

At times $t > \ell_h/c_o$ the entrance pressure wave P_E is subject to multiple reflections from the ends of the hood and partial transmissions into the tunnel. The resulting pressure distribution will first be calculated with neglect of the hood windows and of frictional effects on the train and tunnel walls, and will be denoted by $p_E(x,t)$. This is done by first noting that the characteristic width of the pressure wave front $\sim 2R_h/M$ is large compared to the hood diameter, and therefore that reflections from the open end and reflections and transmission at the junction J can be calculated in the approximation of long wavelength [21].

The following reflection and transmission coefficients are introduced [21,32]:

$$\mathscr{R}_J = \frac{\mathscr{A}_h - \mathscr{A}}{\mathscr{A}_h + \mathscr{A}}, \quad \mathscr{T}_J = \frac{2\mathscr{A}_h}{\mathscr{A}_h + \mathscr{A}}. \tag{6}$$

$\mathscr{R}_J$ determines the amplitude of the wave reflected *back into* the hood produced by a wave incident on J from $x > -\ell_h$, and $\mathscr{T}_J$ determines the amplitude of the corresponding wave transmitted from the hood into the tunnel (into $x < -\ell_h$).

The reflection of wave energy from the open end of the hood can be calculated in the same way. But, in this case it is permissible to neglect losses due to radiation from the open end [21]. A compression wave incident on the end is then reflected as an equal and opposite expansion wave, and vice versa. In addition, however, the reflected wave is retarded by a temporal phase lag $\sim 2\ell_E/c_o$, because the usual long wavelength open end condition of vanishing net pressure must actually be applied at $x = +\ell_E$, so that a wave $f(t-x/c_o)$ incident on the open end from within the hood is reflected as $-f(t+x/c_o-2\ell_E/c_o)$. A corresponding phase lag accompanying reflection and transmission at the junction J was shown in Ref. [21] to be very small (typically smaller than about $0.05R_h/c_o$, see also Section 4.1) and will be ignored.

In terms of these definitions it is easily seen that the resulting net pressure $p_E(x,t)$ within the tunnel is given by:

$$p_E(x,t) \;=\; \mathscr{T}_J\sum_{n=0}^{\infty}(-\mathscr{R}_J)^n P_E\left(t+\frac{x}{c_o}-\frac{2n(\ell_h+\ell_E)}{c_o}\right), \quad x<-\ell_h \tag{7}$$

and in the hood is given by

$$p_E(x,t) \;=\; P_E\left(t+\frac{x}{c_o}\right)+p'_E(x,t), \quad -\ell_h<x<0, \tag{8}$$

where

$$p'_E(x,t)=\sum_{n=1}^{\infty}(-\mathscr{R}_J)^n P_E\left(t+\frac{x}{c_o}-\frac{2n(\ell_h+\ell_E)}{c_o}\right) + \mathscr{R}_J\sum_{n=0}^{\infty}(-\mathscr{R}_J)^n P_E\left(t-\frac{x}{c_o}-\frac{2n(\ell_h+\ell_E)}{c_o}-\frac{2\ell_h}{c_o}\right). \tag{9}$$

The utility of taking $p_E(x,t)$ in the form Eq. (8), where the portal generated pressure wave $P_E(t+x/c_o)$ is explicitly separated from the pressure $p'_E(x,t)$ produced by reflections from the ends of the hood, will become evident in Section 6.

4. Pressure waves generated at the hood-tunnel junction

4.1. Interaction of the train nose with the junction

Two plane waves are generated when the train nose passes the junction J (at $x=-\ell_h$) between the hood and the tunnel. One of these is radiated directly into the tunnel (into $x<-\ell_h$) and will be denoted by $P_{JT}(t+x/c_o)$; the second, $P_{JH}(t-x/c_o)$, is radiated back into the hood, where it subsequently experiences multiple reflections from the ends of the hood and partial transmissions through J into the tunnel. These waves are calculated by the procedure described in Ref. [21], by first introducing a solution $\varphi^*_J(\mathbf{x})$ of Laplace's equation that represents a steady potential flow through the junction from the tunnel to the hood. When the hood length ℓ_h exceeds the diameter $2R_h$, the functional form of φ^*_J in the neighbourhood of J is well approximated by the solution of Laplace's equation obtained by assuming the hood to extend to $x=+\infty$. It is readily determined by numerical integration, and is normalized such that

$$\left.\begin{array}{rcll}\varphi^*_J(\mathbf{x}) & \approx & x+\ell_h-\ell_J & \text{for } x+\ell_h\to-\infty \text{ in the tunnel,}\\ & \approx & \frac{\mathscr{A}}{\mathscr{A}_h}(x+\ell_h) & \text{for } x+\ell_h\gg R_h \text{ in the hood.}\end{array}\right\} \tag{10}$$

The length ℓ_J is the effective 'hydrodynamic length' of the junction; it is shown in Ref. [21] that $\ell_J<0.05R$ when $R_h/R<1.25$, and that ℓ_J does not exceed $0.1R$ until $R_h/R>1.4$. The practical effect of this length is to introduce small phase shifts in $P_{JT}(t+x/c_o)$ and $P_{JH}(t-x/c_o)$ analogous to that produced in $P_E(t+x/c_o)$ (Section 3) by the (much larger) end correction $\ell_E=0.61R_h$. These small phase shifts will be ignored.

The method described in Ref. [21] now supplies the representations for the plane waves in the tunnel:

$$P_{JT}\left(t+\frac{x}{c_o}\right)=\frac{\rho_o U^2}{(1-M^2)}\frac{\mathscr{A}_o}{\mathscr{A}}\left(1+\frac{\mathscr{A}_o}{\mathscr{A}}\right)\frac{\mathscr{T}_J}{2} \times\left\{\int_{-\infty}^{\infty}\frac{\partial\varphi^*_J}{\partial x'}(x',0,z_t)\frac{\partial\mathscr{A}_T}{\partial x'}\left(x'+U\left(t+\frac{x+\ell_h}{c_o}\right)\right)\frac{\mathrm{d}x'}{\mathscr{A}_o}-\frac{\mathscr{A}}{\mathscr{A}_h}\right\}, \quad x<-\ell_h, \tag{11}$$

and in the hood:

$$P_{JH}\left(t-\frac{x}{c_o}\right)=\frac{-\rho_o U^2}{(1-M^2)}\frac{\mathscr{A}_o}{\mathscr{A}_h}\left(1+\frac{\mathscr{A}_o}{\mathscr{A}}\right)\frac{\mathscr{T}_J}{2} \times\left\{\int_{-\infty}^{\infty}\frac{\partial\varphi^*_J}{\partial x'}(x',0,z_t)\frac{\partial\mathscr{A}_T}{\partial x'}\left(x'+U\left(t-\frac{x+\ell_h}{c_o}\right)\right)\frac{\mathrm{d}x'}{\mathscr{A}_o}-\frac{\mathscr{A}}{\mathscr{A}_h}\right\}, \quad -\ell_h<x<0. \tag{12}$$

4.2. The overall junction-generated pressure $p_J(x,t)$

At time $t\sim\ell_h/U+\ell_h/c_o$ the component wave $P_{JH}(t-x/c_o)$ radiated into the hood from the junction is reflected at the open end of the hood. As time progresses further reflections occur from both ends of the hood, and energy is also transmitted into the tunnel (into $x<-\ell_h$). At any instant the net pressure $p_J(x,t)$ produced by the nose-junction interaction and radiated into the tunnel and within the hood can be calculated in terms of P_{JH} and P_{JT} and these multiple reflections by making use of the reflection and transmission coefficients $\mathscr{R}_J$ and $\mathscr{T}_J$ defined in Eq. (6) giving in the tunnel:

$$p_J(x,t)=P_{JT}\left(t+\frac{x}{c_o}\right)-\mathscr{T}_J\sum_{n=0}^{\infty}(-\mathscr{R}_J)^nP_{JH}\left(t+\frac{x}{c_o}-\frac{2n(\ell_h+\ell_E)}{c_o}-\frac{2\ell_E}{c_o}\right),\quad x<-\ell_h \tag{13}$$

and in the hood:

$$p_J(x,t)=\sum_{n=0}^{\infty}(-\mathscr{R}_J)^n\left\{P_{JH}\left(t-\frac{x}{c_o}-\frac{2n(\ell_h+\ell_E)}{c_o}\right)-P_{JH}\left(t+\frac{x}{c_o}-\frac{2n(\ell_h+\ell_E)}{c_o}-\frac{2\ell_E}{c_o}\right)\right\},\quad -\ell_h<x<0. \tag{14}$$

For an unvented hood (no windows) and in the absence of the frictional pressure sources associated with turbulence separation between the tunnel and hood walls and the train, the overall compression wave radiated into the tunnel is equal to $p_E(x,t)+p_J(x,t)$ determined, respectively, by Eqs. (7) and (13).

5. Pressure wave generated by the viscous drag

The frictional drag on the sides of the train and on the tunnel wall are together equivalent to a low frequency dipole source, and are responsible for the contribution p_D to the compression wave. Within the hood and tunnel the flow over the train separates just to the rear of the nose, close to the point labelled S in Fig. 2, and turbulence progressively fills the region between S and the hood portal. The length of this region increases uniformly at the speed U of the train. The dominant contribution to the pressure from the turbulence is manifested by the accompanying surface drag—there is a small additional contribution from the 'exit flow vortex' shown in Fig. 2, but this is small enough to be neglected in comparison with the overall contribution from the interior sources [23]. It was shown in Ref. [23] that p_D is well approximated by

$$p_D(\mathbf{x},t)=-\rho_o\int_{-\infty}^{\infty}\mathrm{d}\tau\oint_{S'}v_*^2(\mathbf{x}',\tau)\frac{\partial G}{\partial x'}(\mathbf{x},\mathbf{x}',t-\tau)\,\mathrm{d}S(\mathbf{x}'), \tag{15}$$

where the surface integral is over those surface sections S' of the train and interior hood and tunnel walls 'wetted' by the separated flow, and $v_*(\mathbf{x}',\tau)$ is the friction velocity on S'. If the front of the train nose is assumed to cross the entrance plane of the hood at $t=0$, the integrand in Eq. (15) is null for $\tau<L/U$.

The pressure p_D grows approximately linearly with time after the formation of the main compression wave front, and is important only well after the nose has entered the hood. The characteristic length scale of this pressure $\sim$ 'wetted length of the train'$/M$, which tends to exceed the length of the hood when the contribution from p_D has become significant. Thus, we can calculate this pressure field by assuming the hood to be acoustically compact. Furthermore, when $\mathbf{x}$ lies within the tunnel the main contributions to the integral in Eq. (15) are from those regions of the tunnel and hood that are not close to either the hood portal E or the junction J (see Fig. 2). We can therefore use the approximations [29,33] for x' in the tunnel:

$$\frac{\partial G}{\partial x'}(\mathbf{x},\mathbf{x}',t-\tau)\approx-\frac{1}{2\mathscr{A}}\left\{\delta\left(t-\tau-\frac{(x-x')}{c_o}\right)+\delta\left(t-\tau+\frac{(x+x'-2\ell_D)}{c_o}\right)\right\} \tag{16}$$

and for x' in the hood:

$$\begin{aligned}\frac{\partial G}{\partial x'}(\mathbf{x},\mathbf{x}',t-\tau)\approx\ &-\frac{1}{2\mathscr{A}_h}\left\{\delta\left(t-\tau-\frac{\{x-\ell_D-(\mathscr{A}/\mathscr{A}_h)(x'-\ell_E)\}}{c_o}\right)\right.\\&\left.+\delta\left(t-\tau-\frac{\{x-\ell_D+(\mathscr{A}/\mathscr{A}_h)(x'-\ell_E)\}}{c_o}\right)\right\},\end{aligned} \tag{17}$$

where

$$\ell_D \;=\; \ell_E + \ell_J - \ell_h\left(1 - \frac{\mathscr{A}}{\mathscr{A}_h}\right) \approx \ell_E - \ell_h\left(1 - \frac{\mathscr{A}}{\mathscr{A}_h}\right). \tag{18}$$

It was shown in Ref. [23] that the collective action of all surface elements of the train and tunnel subject to the turbulence fluctuations produce a predominantly steady drag force per unit surface area. Therefore, for the purpose of evaluating the integral of Eq. (15), it is permissible to assign to the friction velocity $v_*(\mathbf{x}', \tau)$ an appropriate mean value, which is taken to assume different, but constant values on the surfaces of the train and on the tunnel and hood walls. Of course, the total drag increases linearly with time because the length of the turbulent region producing the drag (i.e. the length of the section of the train within the tunnel) is increasing at the speed U of the train.

We therefore set [23]

$$v_* = \mu U_\infty, \tag{19}$$

where μ is a constant and U_∞ is the mean turbulent flow velocity relative to the surface S'. This mean velocity takes different values for the different parts of S', which comprises the sections of the train within the hood and within the tunnel, and the tunnel and hood walls. If the mean flow is assumed to be adiabatic and locally steady we can accordingly introduce the four velocities $U_\infty = U_{TW},\ U_{HW},\ U_{TT},\ U_{HT}$ where [23]

$$\begin{aligned}
U_{TW} &= \frac{\mathscr{A}_o U}{(\mathscr{A} - \mathscr{A}_o)}\left\{1 - \frac{M\mathscr{A}}{(\mathscr{A} - \mathscr{A}_o)} + \frac{M^2\mathscr{A}(2\mathscr{A} - \mathscr{A}_o)}{2(\mathscr{A} - \mathscr{A}_o)^2}\right\} \quad \text{for the tunnel wall,}\\
U_{HW} &= \frac{\mathscr{A}_o U}{(\mathscr{A}_h - \mathscr{A}_o)}\left\{1 - \frac{M\mathscr{A}_h}{(\mathscr{A}_h - \mathscr{A}_o)} + \frac{M^2\mathscr{A}_h(2\mathscr{A}_h - \mathscr{A}_o)}{2(\mathscr{A}_h - \mathscr{A}_o)^2}\right\} \quad \text{for the hood wall,}\\
U_{TT} &= \frac{\mathscr{A} U}{(\mathscr{A} - \mathscr{A}_o)}\left\{1 - \frac{M\mathscr{A}_o}{(\mathscr{A} - \mathscr{A}_o)} + \frac{M^2\mathscr{A}_o(2\mathscr{A} - \mathscr{A}_o)}{2(\mathscr{A} - \mathscr{A}_o)^2}\right\} \quad \text{for the train in the tunnel,}\\
U_{HT} &= \frac{\mathscr{A}_h U}{(\mathscr{A}_h - \mathscr{A}_o)}\left\{1 - \frac{M\mathscr{A}_o}{(\mathscr{A}_h - \mathscr{A}_o)} + \frac{M^2\mathscr{A}_o(2\mathscr{A}_h - \mathscr{A}_o)}{2(\mathscr{A}_h - \mathscr{A}_o)^2}\right\} \quad \text{for the train in the hood.}
\end{aligned} \tag{20}$$

Numerical and experimental results discussed in Ref. [23] indicate that for model scale applications at speeds U up to about 350 km/h, excellent predictions of the drag component p_D of the compression wave pressure are obtained for $\mu \equiv v_*/U_\infty \sim 0.053$ (mistakenly reported as $\mu = 0.047$ in Ref. [23]). However, because of the absence of Reynolds number similarity between full scale and model scale experiments, it must be anticipated that model scale predictions will not necessarily yield entirely satisfactory predictions for the contribution of drag to the overall pressure signature at full scale. Thus, it is advisable that predictions be made for a *range of values* of μ to obtain a range of predictions that can be expected to bound the full scale situation.

Now define

$$p_D(x,t) = p_{DH}(x,t) + p_{DT}(x,t), \tag{21}$$

where $p_{DH},\ p_{DT}$, respectively, denote the components of p_D generated by the turbulence drag within the hood and within the tunnel. Then Eqs. (15)–(17) and (20) yield for $x < -\ell_h$ (in the tunnel) [23]:

$$\begin{aligned}
p_{DH}(x,t) = \frac{\mu^2\rho_o}{2\mathscr{A}_h}(L_{R_h}U_{HW}^2 + L_h U_{HT}^2)\Bigg\{&\left[\left(\frac{U(t + x/c_o) - L - M(\ell_D - \ell_E\mathscr{A}/\mathscr{A}_h)}{1 - M\mathscr{A}/\mathscr{A}_h}\right)_+\right.\\
&\left.-\left(\frac{U(t + x/c_o) - L - M(\ell_D - \ell_E\mathscr{A}/\mathscr{A}_h)}{1 - M\mathscr{A}/\mathscr{A}_h} - \ell_h\right)_+\right]\\
&+\left[\left(\frac{U(t + x/c_o) - L - M(\ell_D + \ell_E\mathscr{A}/\mathscr{A}_h)}{1 + M\mathscr{A}/\mathscr{A}_h}\right)_+\right.\\
&\left.-\left(\frac{U(t + x/c_o) - L - M(\ell_D + \ell_E\mathscr{A}/\mathscr{A}_h)}{1 + M\mathscr{A}/\mathscr{A}_h} - \ell_h\right)_+\right]\Bigg\},
\end{aligned} \tag{22}$$

$$p_{DT}(x,t)=\frac{\mu^2\rho_o}{2\mathscr{A}}\left(L_R U_{TW}^2+L_h U_{TT}^2\right)\left\{\left(\frac{U(t+x/c_o)-L}{1-M}-\ell_h\right)_+ +\left(\frac{U(t+x/c_o)-L-2M\ell_D}{1+M}-\ell_h\right)_+\right\}, \tag{23}$$

where $(x)_+ = xH(x)$, and

$$L_{R_h}=2\pi R_h,\quad L_R=2\pi R,\quad L_h=2\pi h, \tag{24}$$

are the respective perimeters of the hood, tunnel and uniform section of the train.

6. Pressure contribution from the windows

6.1. Direct pressure produced at a window by the passing train

To calculate the influence of hood windows on the formation of the compression wave it is first necessary to calculate the pressure history in the neighbourhood of each window when the contributions from the windows are ignored. This is done using the results of Sections 3–5.

At the kth window (whose centroid is at $x=x_k$, $-\ell_h<x_k<0$) this pressure is the sum of contributions from: (i) P_E and p'_E of Eqs. (1) and (9), produced by the interaction of the train nose with the hood portal and subsequent reflections from the ends of the hood; (ii) the pressure wave p_J of Eq. (14) produced by the interaction of the nose with the junction; and (iii) the hood component p_{DH} of the pressure p_D, Eq. (21), produced by separated flow over the train and tunnel walls:

$$P_E\left(t+\frac{x_k}{c_o}\right)+p'_E(x_k,t)+p_J(x_k,t)+p_{DH}(x_k,t). \tag{25}$$

But this representation is applicable only for times *prior to the arrival of the nose at the window* (i.e. before time $t\sim -x_k/U>0$ measured from the instant at which the train nose crosses the hood entrance plane). As the nose passes the window there is a rapid reduction in the mean pressure by an amount equal to the uniform peak value attained by $P_E(t+x/c_o)$, namely

$$\frac{\rho_o U^2}{(1-M^2)}\frac{\mathscr{A}_o}{\mathscr{A}_h}\left(1+\frac{\mathscr{A}_o}{\mathscr{A}}\right),$$

which is generated ahead of the train by sources distributed over the nose (of length L) that have now passed the window.

The pressure reduction occurs smoothly in practice over a time of order L/U. The pressure variation over the window during the passage of the train nose can be estimated by calculating the 'near field' pressure generated on the hood wall in the vicinity of the nose by the latter's representation in terms of the effective line source

$$\rho_o U^2\left(1+\frac{\mathscr{A}_o}{\mathscr{A}}\right)\frac{\partial}{\partial x}\left[\frac{\partial\mathscr{A}_T}{\partial x}(x+Ut)\delta(y)\delta(z-z_t)\right] \tag{26}$$

distributed on the train axis at the nose [25].

Now the motion near the train nose can be regarded as steady in a reference frame moving with the train, provided the nose is more than a tunnel diameter from the entrance plane of the hood. Then the wall pressure generated by a *point* source $\delta(x-x'+Ut)\delta(y)\delta(z-z_t)$ is easily shown to be given by [30]

$$\frac{1}{\pi^2 R_h\sqrt{1-M^2}}\sum_{n=0}^{\infty}\int_0^{\infty}\frac{\sigma_n I_n(k|z_t|)}{k[I_{n-1}(kR_h)+I_{n+1}(kR_h)]}\cos\left(\frac{k(x-x'+Ut)}{\sqrt{1-M^2}}\right)\mathrm{d}k+\frac{(x-x'+Ut)}{2\mathscr{A}_h(1-M^2)}, \tag{27}$$

where the integral is to be interpreted as a generalized Fourier integral [34] and where (recalling that $I_n(0) \equiv 0$ when $n \geqslant 1$)

$$\sigma_n = \begin{cases} 1, & n = 0, \\ 2, & n \geqslant 1 \text{ and } z_t > 0, \\ 2(-1)^n, & n \geqslant 1 \text{ and } z_t < 0. \end{cases} \tag{28}$$

The second term in Eq. (27) ensures that the pressure vanishes in the region between the source, moving within the hood in the negative x-direction, and the open end of the hood. The two cases $z_t \gtrless 0$ correspond, respectively, to the two cases in which the train track is 'near' the window (as in Fig. 3b) or 'far' from the window.

The corresponding pressure variation at the window at $x = x_k$ during the passage of the train nose can now be calculated by convolving expression (27) with the train nose source (26). The actual net pressure fluctuation at the window produced by the entrance wave component P_E of expression (25) can then be cast in the form

$$P_E\left(t + \frac{x_k}{c_o}\right)\left\{1 - \int_{-\infty}^{\infty} \frac{\mathscr{A}_T(x')}{\mathscr{A}_o}\,\Psi(Ut + x_k - x', z_t)\,\mathrm{d}x'\right\}, \tag{29}$$

where

$$\Psi(x, z_t) = \frac{1}{\pi R_h\sqrt{1 - M^2}} \sum_{n=0}^{\infty} \int_0^{\infty} \frac{\sigma_n \lambda I_n(\lambda|z_t|/R_h)}{I_{n-1}(\lambda) + I_{n+1}(\lambda)} \cos\left(\frac{\lambda x}{R_h\sqrt{1 - M^2}}\right) \mathrm{d}\lambda. \tag{30}$$

The function $\Psi(x, z_t)$ has the characteristics of a 'broadened' δ-function, and satisfies $\int_{-\infty}^{\infty} \Psi(x, z_t)\,\mathrm{d}x = 1$. It is plotted in Fig. 4a for $z_t/R_h = 0, \pm 0.4$ for $M = 0.294$ ($U = 360\,\mathrm{km/h}$), where it is seen to attain a maximum

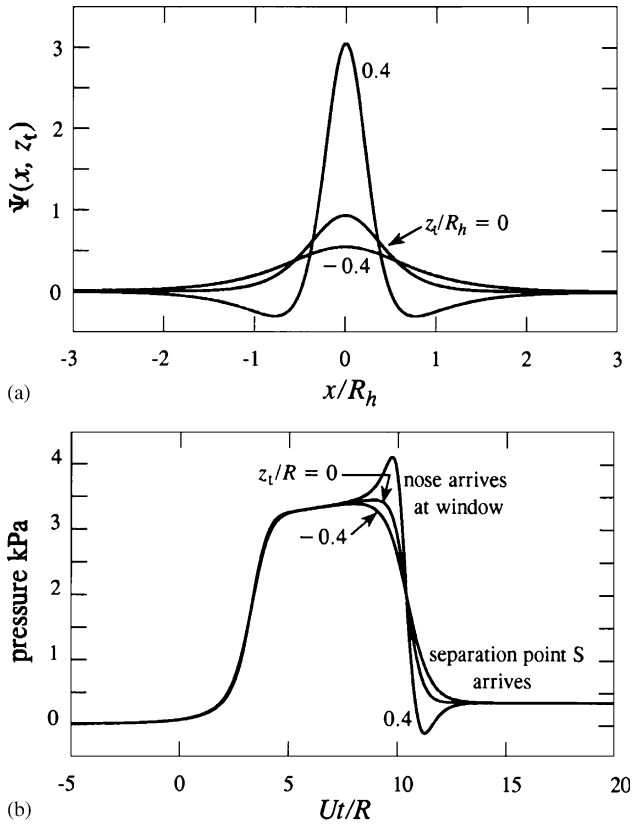

Fig. 4. (a) Illustrating the function $\Psi(x, z_t)$ for the three cases $z_t/R_h = -0.4,\ 0,\ +0.4$ when $M = 0.294$ ($U = 360\,\mathrm{km/h}$); (b) the direct pressure $p'_I(x_k, t)$ defined by Eq. (32) incident on a window whose centroid is at $x_k = -10R$ produced by the passage of the axisymmetric train defined by Eqs. (33) and (34) with $L/h = 3$, $\mathscr{A}_o/\mathscr{A} = 0.2$, $U = 360\,\mathrm{km/h}$ when $R_h = R$, for the three track offsets $z_t/R = 0, \pm 0.4$.

at $x=0$ and to be small for $|x|>2R_h$; $\Psi(x,z_t)\geqslant 0$ for $z_t\leqslant 0$, but has small negative 'wings' for $z_t>0$, the case shown in Fig. 3b where the track runs close to the window.

The integrated term in Eq. (29) is zero until the train nose approaches the kth window at $t\sim -x_k/U$; after the nose has passed the window ($t>(-x_k+L)/U$) the value of the integral tends rapidly to 1, and the pressure represented by Eq. (29) drops to zero. In addition, however, it is also necessary to modify the contribution $p_{DH}(x_k,t)$ in Eq. (25) produced by the surface friction. After the nose has passed the window $p_{DH}(x_k,t)$ must be replaced by its value at $x=x_k,\ t=(-x_k+L)/U$, and remain equal to this until retarded times after the tail of the train has entered the tunnel, because the pressure rise produced by the wake drag on the train and tunnel surfaces lying between the window and the hood entrance must be constant until the tail enters the hood. Hence, in summary, the net 'direct' pressure field $p_I(x_k,t)$, say, that is incident on the kth window at $x=x_k$ when the contribution from the windows is ignored, can be cast in the form

$$p_I(x_k,t)=p'_I(x_k,t)+p'_E(x_k,t)+p_J(x_k,t), \tag{31}$$

where

$$\begin{aligned} p'_I(x_k,t)=P_E\left(t+\frac{x_k}{c_o}\right)\left\{1-\int_{-\infty}^{\infty}\frac{\mathscr{A}_T(x')}{\mathscr{A}_o}\,\Psi(Ut+x_k-x',z_t)\,\mathrm{d}x'\right\}\\ +\begin{cases} p_{DH}(x_k,t), & t<\frac{(-x_k+L)}{U},\\ p_{DH}\left(x_k,\frac{(-x_k+L)}{U}\right), & t>\frac{(-x_k+L)}{U}. \end{cases} \end{aligned} \tag{32}$$

Fig. 4b depicts typical pressure histories of $p'_I(x_k,t)$ at a window whose centroid is at $x_k=-10R$ for the particular case in which the tunnel and hood radii are equal, $U=360\,\mathrm{km/h}$ ($M=0.294$), and $z_t/R=0,\pm 0.4$. The train has been assumed to have an ellipsoidal nose shape defined by

$$r=h\sqrt{\frac{x}{L}\left(2-\frac{x}{L}\right)},\quad 0<x<L\quad \left(r=\sqrt{y^2+z^2}\right). \tag{33}$$

Thus, if s denotes distance from the front of the train, then (ignoring the rear end of the train)

$$\frac{\mathscr{A}_T(s)}{\mathscr{A}_o}=\begin{cases} \frac{s}{L}\left(2-\frac{s}{L}\right), & 0<s<L,\\ 1, & s>L, \end{cases} \tag{34}$$

where $\mathscr{A}_o=\pi h^2$. For the results shown in Fig. 4b it is assumed that

$$\frac{L}{h}=3,\quad \frac{\mathscr{A}_o}{\mathscr{A}}=0.2.$$

Referring to Fig. 4b: the compression wave front arrives at the window at $t\sim 10R/c_o$ or $Ut/R\sim 10M\approx 2.9$; the nose arrives at $Ut/R=10$. There are small differences (not noticeable in the figure) in the shapes of wave front pressure profiles for $z_t=0$ and $z_t=\pm 0.4$, because the time scale of the interaction of the train nose with the hood portal is marginally smaller when $z_t\neq 0$. For $z_t\leqslant 0$ the component of $p'_I(x_k,t)$ produced by the entrance wave P_E (the first line of Eq. (32)) begins to fall as the nose section approaches and passes the window—the fall is complete at $Ut/R\approx 10+L/R=11.34$ when $z_t=0$. When the track offset $z_t/R=0.4$, so that the train passes close to the window, the entrance wave contribution initially increases as the front of the nose approaches the window and becomes temporarily negative during passage of the rear end of the nose. In all cases the pressure p'_I subsequently remains equal to the constant pressure difference ($\sim 0.35\,\mathrm{kPa}$) produced by the frictional drag acting on the sections of the train and hood (of fixed length) between the window and the hood entrance plane.

6.2. Jet formation at the windows

A window behaves as a pressure node at very low frequencies, at which an incident pressure rise within the tunnel is opposed by the production of an equal and opposite expansion wave which propagates away from the window in both directions within the tunnel. The situation is different, however, at the higher frequencies

associated with a compression wave front or the direct pressure p_I' produced by a passing train, when the inertial reaction of air forced through a window becomes significant [22,25]. The pressure fluctuations produced by the compression wave have a time scale $\sim 2R_h/U$, and the corresponding

$$\text{compression wave front thickness } \sim 2R_h/M \approx 6R_h.$$

This is typically much larger than a window diameter, so that the local tunnel pressure may be assumed to be uniform over the inner face of the window. We shall assume this is also a good approximation for the pressure variations p_I' produced by the passing train. The air flow through the windows can then be calculated using model equations proposed by Cummings for circular apertures [25,35,36].

Let $V_k(t)$ denote the mean jet velocity directed *out* of the hood in the plane of the kth window, whose centroid is at $x = x_k$. Because the characteristic acoustic wavelength $\gg R_h$, the volume flow from the window generates two equal plane acoustic waves propagating in both directions away from the window within the hood. Before these waves interact with the ends of the hood or with any other windows they produce a pressure fluctuation within the hood equal to

$$-\frac{\rho_o c_o A_k}{2\mathscr{A}_h}\, V_k\left(t-\frac{|x-x_k|}{c_o}\right). \tag{35}$$

If we temporarily continue to ignore the interaction of these waves with the other windows, we can easily determine the net pressure field they produce within the hood ($-\ell_h < x < 0$) and in the tunnel ($x < -\ell_h$) by taking account of multiple reflections from the ends of the hood and transmissions into the tunnel. If this net pressure field is denoted by p_k, we find that in the tunnel:

$$\begin{aligned} p_k(x,t) = & -\frac{\rho_o c_o A_k}{2\mathscr{A}_h}\mathscr{T}_J \sum_{n=0}^{\infty}(-\mathscr{R}_J)^n\left\{V_k\left(t+\frac{\{x-x_k-2n(\ell_h+\ell_E)\}}{c_o}\right)\right. \\ & \left. - V_k\left(t+\frac{\{x+x_k-2n(\ell_h+\ell_E)-2\ell_E\}}{c_o}\right)\right\} \end{aligned} \tag{36}$$

and in the hood:

$$\begin{aligned} p_k(x,t) = & -\frac{\rho_o c_o A_k}{2\mathscr{A}_h}\, V_k\left(t-\frac{|x-x_k|}{c_o}\right) \\ & -\frac{\rho_o c_o A_k}{2\mathscr{A}_h}\sum_{n=0}^{\infty}(-\mathscr{R}_J)^n\left\{-V_k\left(t+\frac{\{x+x_k-2n(\ell_h+\ell_E)-2\ell_E\}}{c_o}\right)\right. \\ & + \chi_n V_k\left(t+\frac{\{x-x_k-2n(\ell_h+\ell_E)\}}{c_o}\right)+\chi_n V_k\left(t+\frac{\{-x+x_k-2n(\ell_h+\ell_E)\}}{c_o}\right) \\ & \left. +\mathscr{R}_J V_k\left(t-\frac{\{x+x_k+2n(\ell_h+\ell_E)+2\ell_h\}}{c_o}\right)\right\}, \end{aligned} \tag{37}$$

where

$$\chi_n = \begin{cases} 0, & n=0, \\ 1, & n\geqslant 1. \end{cases} \tag{38}$$

6.3. Overall contribution to the compression wave by the windows

The overall component $p_W(x,t)$ ($x < -\ell_h$) of the compression wave transmitted into the tunnel attributable to N windows may now be determined from the following self-consistent system of equations

$$p_W(x,t) = \sum_{k=1}^{N} p_k(x,t), \tag{39}$$

where $p_k(x,t)$ is defined for the kth window as in Eq. (36), and the V_k are determined by the following system of Cummings' equations [35,36]:

$$\left.\begin{array}{rcl} \bar{\ell}_k(t)\rho_o \frac{\mathrm{d}V_k}{\mathrm{d}t} + \frac{\rho_o V_k|V_k|}{2\sigma^2} &=& p_I(x_k,t) + \sum_{j=1}^{N} p_j(x_k,t) \\ \frac{d\mathscr{L}_k}{dt} &=& |V_k(t)| \\ \bar{\ell}_k(t) &=& \frac{\pi R_k}{4} + \left(\ell_w + \frac{\pi R_k}{4}\right) \Big/ \left[1 + \frac{1}{3}\left(\frac{\mathscr{L}_k}{2R_k}\right)^{1.585}\right] \end{array}\right\}, \quad k = 1,\ 2, \ldots N, \tag{40}$$

where each $p_j(x_k,t)$ $(-\ell_h < x_k < 0)$ is given by Eq. (37), and $p_I(x,t)$ is defined by Eq. (31). The constant σ is the effective jet contraction ratio, which to a good approximation can be assumed to be constant and equal to 0.75; $\mathscr{L}_k$ is the axial length of the jet exhausting from the kth window, and $R_k = \sqrt{A_k/\pi}$ is the equivalent radius of the kth window (see Refs. [25,35,36] for further details). The *causal* solution of these equations is required, subject to $V_k(t) = 0$, $\mathscr{L}_k(t) = 0$ $(k = 1, 2, \ldots, N)$ for t large and negative; $\mathscr{L}_k(t)$ should be reset to zero if and when V_k changes sign.

7. The compression wave in the tunnel

7.1. Representation in terms of calculated components

The results of the calculations described in Sections 3–6 may now be combined to yield the following prediction for the plane compression wave $p(t + x/c_o)$ within the tunnel $(x < -\ell_h)$:

$$p\left(t + \frac{x}{c_o}\right) = p_E(x,t) + p_J(x,t) + p_D(x,t) + p_W(x,t) \quad (x < -\ell_h), \tag{41}$$

where the pressure components on the right and their respective sources are summarized in Table 1.

7.2. Wave generation in the absence of windows and hood

Typical laboratory scale measurements of the compression wave generated when a train enters a tunnel without a hood and without windows are displayed in Fig. 5 (△). The experiment was performed at the Railway Technical Research Institute in Tokyo (RTRI) using apparatus described in Ref. [22]. The tunnel consisted of a 6.5 m long, thin-walled, circular cylindrical tube of internal radius $R = 50$ mm. A model axisymmetric 'train' with an ellipsoidal nose profile defined as in Eqs. (33) and (34) was projected into the tunnel at $U = 349$ km/h $(M = 0.285)$ and guided by a wire stretched along the tunnel axis and passing smoothly through a cylindrical bore hole along the train axis. The uniform train cross-section $\mathscr{A}_o$ and the nose dimensions are given by

$$\mathscr{A}_o = \pi h^2, \quad h = 22.35\,\mathrm{mm}, \quad L = 67.05\,\mathrm{mm}, \tag{42}$$

so that the blockage $\mathscr{A}_o/\mathscr{A} \approx 0.2$ $(\mathscr{A} = \pi R^2)$. The tail of the model train had an identical ellipsoidal shape, and the overall length of the train was 1239 mm.

The front of the nose crosses the entrance plane of the tunnel at time $t = 0$, and the pressure wave was measured within the tunnel at a distance $\ell_m = 1.5$ m from the entrance. In the Fig. 5 the pressure at $x = -\ell_m$ is

Table 1
Compression wave constituents

Component	Formula	Source
p_E	(7)	Interaction of the train nose with the hood portal
p_J	(13)	Interaction of the nose with the junction
p_D	(21)	Turbulent drag on the train and tunnel/hood wall
p_W	(39)	The hood windows

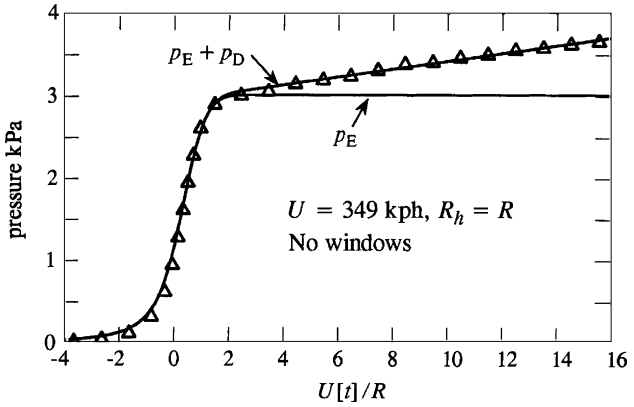

Fig. 5. Measured (△) and predicted compression wave profiles in the absence of a hood and windows, for a model scale ellipsoidal nose train defined by Eqs. (33), (34) and (42) entering a circular cylindrical tunnel of radius $R = 50\,\text{mm}$ at $U = 349\,\text{km/h}$ when $z_t = 0$. The overall predicted pressure $= p_E + p_D$; the main pressure rise at the wavefront is determined by the component p_E produced by the interaction of the train nose with the tunnel portal; the linearly increasing 'tail' to the rear of the wave front is governed by the turbulence generated pressure p_D.

plotted against $U[t]/R$, where $[t] = t - \ell_m/c_o$ is the retarded time. The pressure rise begins just before the nose enters the tunnel at $U[t]/R = 0$. For this case the theoretically predicted pressure is attributed to the components p_E and p_D of Table 1. The separate pressure rise produced by p_E, which is generated by the interaction of the nose with the tunnel entrance, controls the principal characteristics of the wave front; as indicated in the figure p_E becomes constant (equal to the value given in Eq. (4)) at $U[t]/R \sim 2$. The subsequent approximately linear increase with distance behind the front is determined by the component p_D produced by the turbulence drag. The predicted rate of this growth for given train speed U depends on the value of the friction coefficient μ (see Eq. (19)). The values of μ appropriate for model scale tests and at full scale are unlikely to be equal because of the overall absence of Reynolds number similarity, and because of the very significant differences in the effective surface roughness at model and full scale. For the present calculation it is assumed that $\mu = 0.053$.

7.3. Wave generation in an unvented hood

The compression wave produced in a hood with no windows consists of the combination $p_E + p_J + p_D$, corresponding to separate contributions from the interaction of the train nose with the hood portal and the junction between the hood and tunnel, and from the turbulence drag sources. Fig. 6 illustrates a comparison of theory and experiment for a hood with the dimensions

$$\ell_h = 10R, \quad R_h = 1.25R \quad (\mathscr{A}_h/\mathscr{A} = 1.5625) \tag{43}$$

and the ellipsoidal nose train defined by Eqs. (33), (34) and (42) when

$$U = 301\,\text{km/h}, \quad z_t = 0.4R, \quad (M \sim 0.245).$$

In the figure are shown both the pressure p and the pressure 'gradient' $\partial p/\partial t$. The latter is important because it determines the subjective effect of the pressure wave within the tunnel, and is also proportional to the amplitude of the sound that would be radiated from the distant tunnel exit (the 'micro-pressure wave') in the absence of nonlinear wave steepening. The agreement between measurement and theory (for $\mu = 0.053$) is maintained up to about $U[t]/R = 14$, after which the measured pressure falls off because of the imminent arrival of the train tail at the hood portal.

A detailed analysis is given in Ref. [21] of the role of multiple reflections within the hood in producing the 'rippled' pressure profile and the 'pulsatile' pressure gradients shown in Fig. 6. It will suffice to note here that in evaluating the infinite series (with respect to the subscript n) in the various representations of p_E, p_J and p_W, only terms up to and including $n = N_{\max} \equiv 6$ have been retained. To justify this, observe that the train nose crosses the hood in time $\sim \ell_h/U$ and the formation of the wave front is complete at time $\sim 2\ell_h/U$ after the

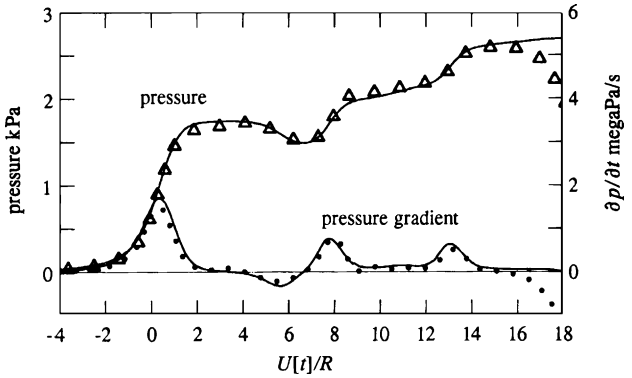

Fig. 6. Predictions of the compression wave pressure and pressure gradient (——) compared with experiment (△, •) for a model scale ellipsoidal nose train defined by Eqs. (33), (34) and (42) entering at $U = 301\,\mathrm{km/h}$ a circular cylindrical tunnel with an unvented hood when $R = 50\,\mathrm{mm}$, $R_h = 1.25R$, $\ell_h = 10R$, $z_t = 0.4R$.

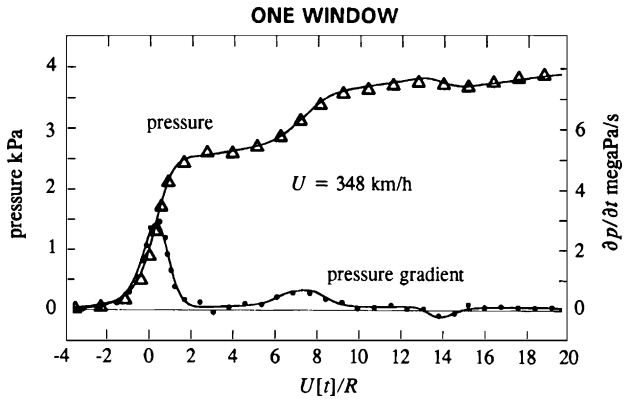

Fig. 7. Measured (△, •) and predicted (——) compression wave pressure and pressure gradient when $R_h = R$, $\ell_w = 0.1R$, $z_t = 0$ for the model scale train defined by Eqs. (33), (34) and (42) when $U = 348\,\mathrm{km/h}$, $\ell_x = \ell_\theta = 0.4R$, $x_1 = -10R$ and $\mu = 0.053$. Measurements are made within the tunnel at a distance of 1.5 m from the hood entrance plane.

nose enters the hood. During this latter time interval sound travels a distance $\sim 2\ell_h/M$, corresponding to $N_{\max}\sim 1/M\sim 4$ round trips within the hood.

7.4. *Influence of one window when $R_h = R$*

Model scale experiments performed at RTRI used hoods with (curvilinear) rectangular windows orientated as indicated in Fig. 3a, with sides of lengths ℓ_x, ℓ_θ, respectively, in the x-direction and in the azimuthal direction. In this section we compare predictions and measurements for a hood of radius $R_h = R$ and wall thickness $\ell_w = 0.1R$, having one window of area $A_1 = \ell_x\ell_\theta$ at $x_1 = -10R$ when the train enters along the tunnel axis. In the absence of a junction the predicted compression wave pressure $= p_E + p_D + p_W$.

Fig. 7 displays measured values (△, •) previously reported in Refs. [22,25] and predictions (——) of the compression wave pressure and pressure gradient for the model train of Eqs. (33), (34) and (42) when

$$\ell_x = \ell_\theta = 0.4R \quad (A_1/\mathscr{A} = 0.051), \quad U = 348\,\mathrm{km/h}, \quad \mu = 0.053. \tag{44}$$

The various interactions that control the nonuniform pressure rise across the wave front have been discussed in Refs. [22,25], to which the reader is referred for details. It is merely necessary to note the overall agreement between theory and experiment furnished by Cummings' [35,36] equations governing jet formation in the

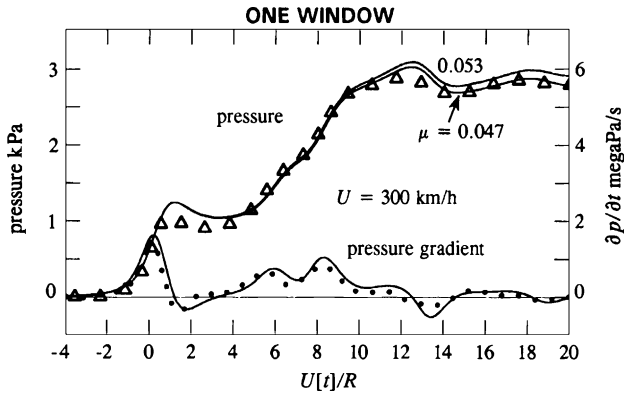

Fig. 8. Measured (△, •) and predicted (——) compression wave pressure and pressure gradient when $R_h = R$, $\ell_w = 0.1R$, $z_t = 0$ for the model scale train defined by Eqs. (33), (34) and (42) when $U = 300\,\mathrm{km/h}$, $\ell_x = 1.6R$, $\ell_\theta = 0.4R$, $x_1 = -10R$, for the two cases $\mu = 0.047,\ 0.053$. Measurements are made within the tunnel at a distance of 1.5 m from the hood entrance plane.

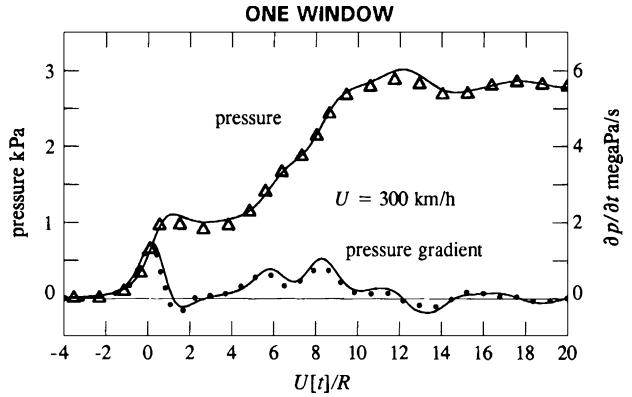

Fig. 9. Measured (△, •) and predicted (——) compression wave pressure and pressure gradient when $R_h = R$, $\ell_w = 0.1R$, $z_t = 0$ for the model scale train defined by Eqs. (33), (34) and (42), with $U = 300\,\mathrm{km/h}$, $\mu = 0.047$, when the single window of dimensions $\ell_x = 1.6R$, $\ell_\theta = 0.4R$ at $x_1 = -10R$ is modelled by two windows at $x_1 = -9.8R$, $x_2 = -10.2R$ each of dimensions $\ell_x = 0.8R$, $\ell_\theta = 0.4R$. Measurements are made within the tunnel at a distance of 1.5 m from the hood entrance plane.

window. The predicted amplitude of the pressure at later times ($U[t]/R > 8$) includes a significant contribution from the turbulence drag component p_D, whose magnitude depends on the value of the wall friction coefficient μ.

An interesting problem emerges with increasing axial length of the window. Figs. 8 and 9 are for the case

$$x_1 = -10R, \quad \ell_x = 1.6R, \quad \ell_\theta = 0.4R \quad (A_1/\mathscr{A} = 0.204), \quad U = 300\,\mathrm{km/h}. \tag{45}$$

The axial length of the window is now comparable with the tunnel diameter, and it might be expected that a naive model that replaces the window by a circular aperture of equal area at its centroid will yield poor agreement with experiment. In fact it can be seen from results shown in Fig. 8 that the overall predictions are still reasonable, but when the friction coefficient $\mu = 0.053$ the predicted pressure at later times ($U[t]/R > 8$) is too large. Now the 'pressure release' provided by a long, 'slit-like' window would tend to reduce the mean frictional pressure gradient along the sides of the passing train. It can therefore be argued that a smaller value of μ would be more representative of the actual flow. Results in Fig. 8 reveal that a modest 10% reduction to $\mu = 0.047$ greatly improves the agreement with experiment at large times. This change has a negligible effect on the pressure gradient $\partial p/\partial t$.

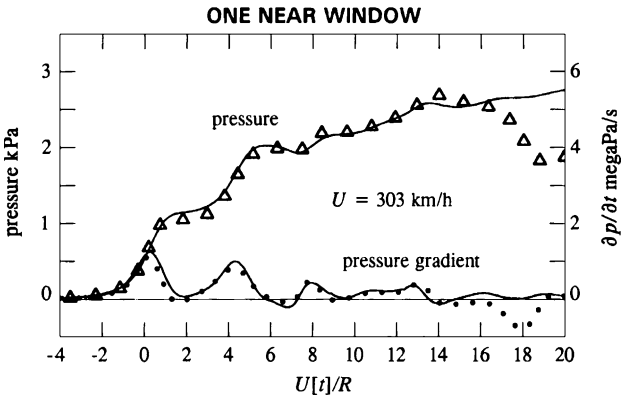

Fig. 10. Measured (△, •) and predicted (——) compression wave pressure and pressure gradient when $R_h = 1.25R$, $\ell_w = 0.06R$, $z_t = 0.4R$ for the model scale train defined by Eqs. (33), (34) and (42), with $U = 303\,\mathrm{km/h}$, $\mu = 0.053$, when the single window of dimensions $\ell_x = 1.2R$, $\ell_\theta = 0.4R$ at $x_1 = -5R$ is modelled by three windows at $x_1 = -4.6R$, $x_2 = -5R$, $x_3 = -5.4R$ each of dimensions $\ell_x = 0.4R$, $\ell_\theta = 0.4R$. Measurements are made within the tunnel at a distance of 1.5 m from the hood entrance plane.

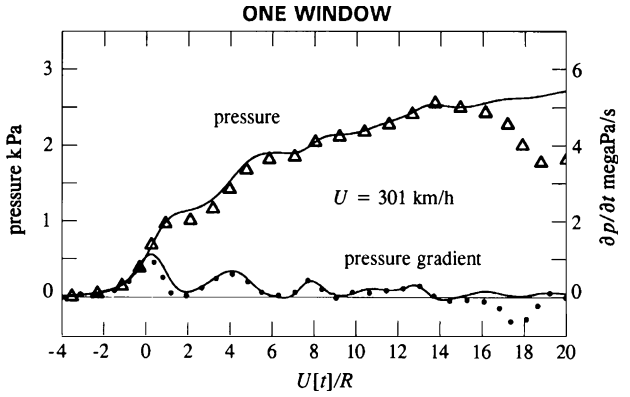

Fig. 11. Measured (△, •) and predicted (——) compression wave pressure and pressure gradient when $R_h = 1.25R$, $\ell_w = 0.06R$, $z_t = 0$ for the model scale train defined by Eqs. (33), (34) and (42), with $U = 301\,\mathrm{km/h}$, $\mu = 0.053$, when the single window of dimensions $\ell_x = 1.2R$, $\ell_\theta = 0.4R$ at $x_1 = -5R$ is modelled by three windows at $x_1 = -4.6R$, $x_2 = -5R$, $x_3 = -5.4R$ each of dimensions $\ell_x = 0.4R$, $\ell_\theta = 0.4R$. Measurements are made within the tunnel at a distance of 1.5 m from the hood entrance plane.

A further overall improvement in the agreement of theory and experiment is achieved by modelling the window of dimensions $\ell_x = 1.6R$, $\ell_\theta = 0.4R$ by two adjacent windows each of dimensions $\ell_x = 0.8R$, $\ell_\theta = 0.4R$. This is illustrated in Fig. 9, where we have taken

$$x_1 = -9.8R,\ x_2 = -10.2R \quad (\mathscr{A}_1/\mathscr{A} = A_2/\mathscr{A} = 0.102), \quad \mu = 0.047. \tag{46}$$

7.5. *One window when $R_h = 1.25R$ and $z_t \neq 0$*

Figs. 10–12 depict comparisons of theory and experiment for a hood of length $\ell_h = 10R$ and radius $R_h = 1.25R$ having one window at $x_1 = -5R$. The window has the dimensions $\ell_x = 1.2R$, $\ell_\theta = 0.4R$ and is modelled theoretically by three adjacent windows each of dimensions $\ell_x = 0.4R$, $\ell_\theta = 0.4R$. The three figures illustrate the influence of track offset, being, respectively, for $z_t = 0.4R$, 0, $-0,4R$ and $U = 303$, 301, 302 km/h ($M \sim 0.25$). It is interesting to note that both theory and experiment indicate that the magnitude of the first, subjectively important peak in the pressure gradient assumes larger values for both positive *and negative* values of the track displacement z_t.

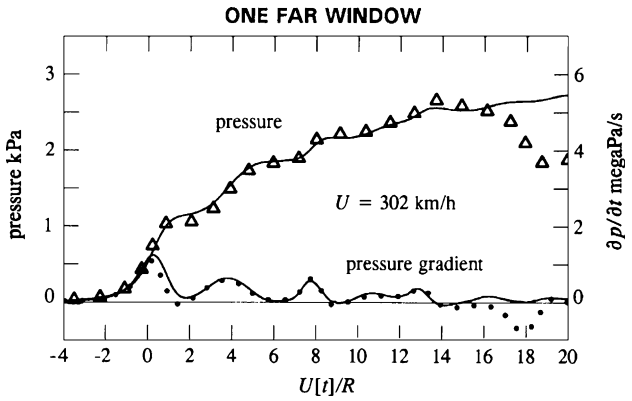

Fig. 12. Measured (△, •) and predicted (——) compression wave pressure and pressure gradient when $R_h = 1.25R$, $\ell_w = 0.06R$, $z_t = -0.4R$ for the model scale train defined by Eqs. (33), (34) and (42), with $U = 302\,\text{km/h}$, $\mu = 0.053$, when the single window of dimensions $\ell_x = 1.2R$, $\ell_\theta = 0.4R$ at $x_1 = -5R$ is modelled by three windows at $x_1 = -4.6R$, $x_2 = -5R$, $x_3 = -5.4R$ each of dimensions $\ell_x = 0.4R$, $\ell_\theta = 0.4R$. Measurements are made within the tunnel at a distance of 1.5 m from the hood entrance plane.

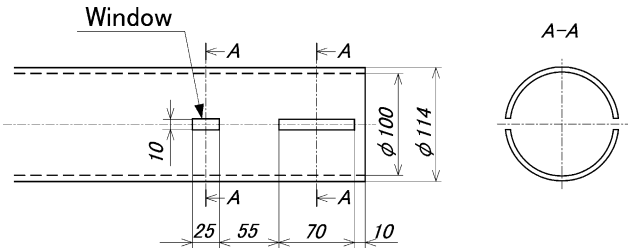

Fig. 13. Schematic arrangement of multiple facing windows in experiments performed for $R_h = R$. Measurements are made within the tunnel at a distance of 1 m from the hood entrance plane.

8. Multiple facing windows

Fig. 13 illustrates one of several experimental configurations used in a series of experiments with circular cylindrical tunnels and hoods of equal radius ($R_h \equiv R$). The 'hood' section close to the portal contains two sets of equal and diametrically opposite windows, one arranged as in our original analytical model of Fig. 3, the second set being the mirror image in the xy-plane. It is evidently a trivial matter to modify the window-jet equations of Section 6 to incorporate these more general arrangements. The tunnel radius $R = 50\,\text{mm}$ and the wall thickness $\ell_w = 0.14R$, and the pressure was measured within the tunnel at 1 m from the entrance plane. The model train had the ellipsoidal nose (and tail) defined in Eqs. (33), (34) and (42), and was projected into the tunnel along the axis of symmetry ($z_t = 0$).

For the case shown in Fig. 13 there are four facing windows; for each set

$$\left.\begin{aligned} &\ell_x = 1.4R,\ \ell_\theta = 0.2R, \quad \text{at } x_1 = -0.9R \\ &\ell_x = 0.5R,\ \ell_\theta = 0.2R, \quad \text{at } x_2 = -2.95R. \end{aligned}\right\}. \tag{47}$$

It might be argued that our analytical model is not really applicable in this case, involving the relatively large, facing windows of dimensions $\ell_x = 1.4R$, $\ell_\theta = 0.2R$ with centroids at a distance of $0.9R$ from the entrance plane. Indeed, the theory implicitly requires that the minimum distance between the first window and the entrance plane should be at least of the order of the hood diameter, so that the motion produced in the hood by flow out of the window can be considered to be uniform and axial near the entrance plane. Nevertheless, predictions agree remarkably well with experiment (Fig. 14), presumably because the mirror-image arrangement causes a rapid alignment of the window flows with the tunnel axis.

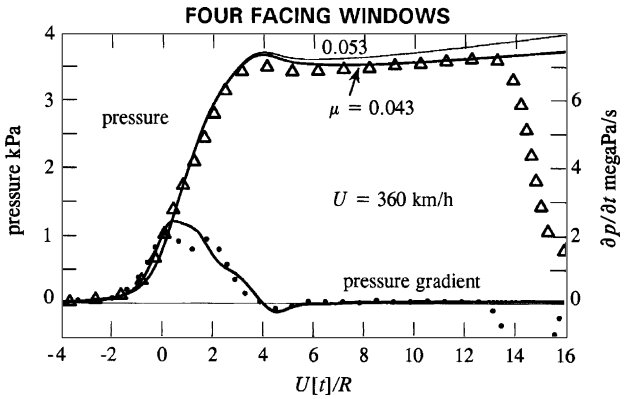

Fig. 14. Measured (△, •) and predicted (——) compression wave pressure and pressure gradient for the case illustrated in Fig. 13: $R_h = R$, $\ell_w = 0.14R$, $z_t = 0$ for the model scale train defined by Eqs. (34) and (42), with $U = 360\,\mathrm{km/h}$ when $\mu = 0.053$ and 0.043. The window arrangement and dimensions are given in Eqs. (47) and (48). Measurements are made within the tunnel at a distance of 1 m from the hood entrance plane.

The comparison with experiment has been performed by modelling the large window in Eq. (47) by three smaller windows, i.e. by the theoretical distribution:

$$\left.\begin{aligned} &\ell_x = 0.467R,\ \ell_\theta = 0.2R, \quad \text{at } x_1 = -0.433R\\ &\ell_x = 0.467R,\ \ell_\theta = 0.2R, \quad \text{at } x_2 = -0.9R\\ &\ell_x = 0.467R,\ \ell_\theta = 0.2R, \quad \text{at } x_3 = -1.367R\\ &\ell_x = 0.5R,\ \ell_\theta = 0.2R, \quad \text{at } x_4 = -2.95R, \end{aligned}\right\}. \tag{48}$$

In Fig. 14 are shown predictions and experiment for $U = 360\,\mathrm{km/h}$, for the two values 0.043 and 0.053 of the friction coefficient μ. It has already been argued that the presence of long or multiple windows will tend to reduce the pressure gradient in the turbulent flow along the sides of the train, and therefore that a reduced value of μ (0.043 in the figure) may be appropriate in these circumstances. It is clear from results shown in Fig. 14 that this is true for the present case at later times ($U[t]/R > 4$), following the main pressure rise across the compression wave front. The overall agreement between theory and experiment is good; the differences in measured and predicted peak values of $\partial p/\partial t$ (generated just as the nose enters the hood) probably occur because the first pair of windows is actually very close to the entrance plane of the hood where the hypothesis of one dimensional acoustics becomes questionable.

9. Measurements at $U = 425\,\mathrm{km/h}$

Fig. 15 depicts schematically the model scale, circular cylindrical hoods designated Cases 1 and 2 that were used in a recent series of experiments performed by Iida and Sakuma [37] at $U \approx 425\,\mathrm{km/h}$ when $R_h = 1.25R$. These tests are the first to be performed at train Mach numbers as large as $M \sim 0.35$. The hood contains one set of windows configured as in Fig. 3. The tunnel radius $R = 50\,\mathrm{mm}$, wall thickness $\ell_w = 0.06R$, and pressure signatures were measured within the tunnel at 1.5 m from the hood entrance plane. The ellipsoidal nose train defined in Eqs. (33), (34) and (42) was projected into the tunnel along $z_t \approx \pm 0.4R$.

In Case 1 the window consists of a single, long slit of length $\ell_x = 9.6R$ and azimuthal width $\ell_\theta = 0.4R$; it occupies most of the length of the hood, beginning just inside the hood portal at a distance of $0.2R$ from the entrance plane. This case evidently poses a stringent test of the robustness of the theory; the window has been modelled by 10 adjacent rectangular windows. The more conventional arrangement of four evenly spaced rectangular windows in Case 2 corresponds more with the hypotheses of the theory, and the results in this case will indicate the ability of the theory to make predictions at high Mach number.

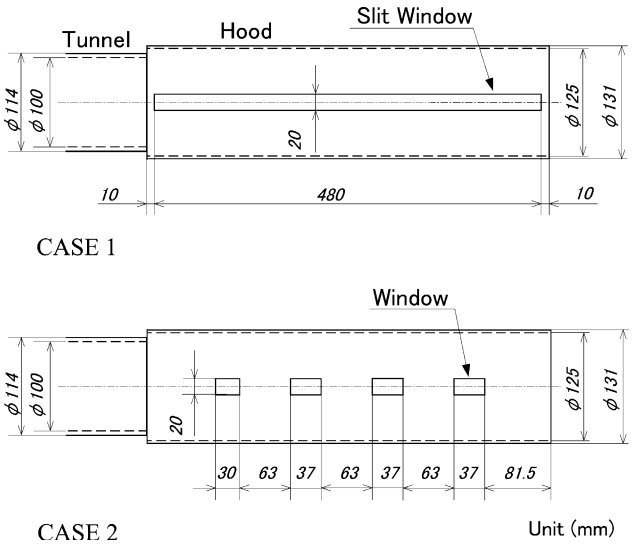

Fig. 15. Side view of the hood with windows arranged as in Fig. 3 for experiments performed by Iida and Sakuma [37] for $R_h = 1.25R$ and $U \approx 425\,\mathrm{km/h}$. Measurements are made within the tunnel at a distance of 1.5 m from the hood entrance plane.

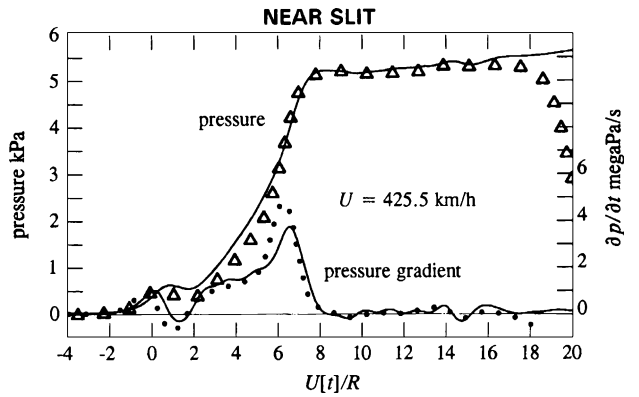

Fig. 16. Measured (△, •) and predicted (——) compression wave pressure and pressure gradient for Case 1 of Fig. 15: $R_h = 1.25R$, $\ell_w = 0.06R$, $z_t = 0.4R$ for the model scale train defined by Eqs. (33), (34) and (42), with $U = 425.5\,\mathrm{km/h}$ when $\mu = 0.047$. The slit window and its modelling by 10 equal rectangular windows are defined in Eqs. (49) and (50). Measurements are made within the tunnel at a distance of 1.5 m from the hood entrance plane.

9.1. Case 1

The slit of dimensions

$$\ell_x = 9.6R, \quad \ell_\theta = 0.4R, \quad \text{occupies the interval } -9.8R < x < -0.2R. \tag{49}$$

It is modelled analytically by 10 equal windows, defined by

$$\ell_x = 0.96R,\ \ell_\theta = 0.4R, \quad \text{at } x_j = -(0.96j - 0.46)R, \quad j = 1,\ 2, \ldots 10. \tag{50}$$

The comparisons in Figs. 16 and 17 are, respectively, for

$$U = 425.5\,\mathrm{km/h}, \quad z_t = 0.4R; \quad U = 426\,\mathrm{km/h}, \quad z_t = -0.4R.$$

In both experiments we have taken $\mu = 0.047$; these are cases where (as already argued above) a reduced value of the friction coefficient μ is appropriate. The accord between theory and experiment must be regarded as very satisfactory, especially in view of the size and disposition of the window.

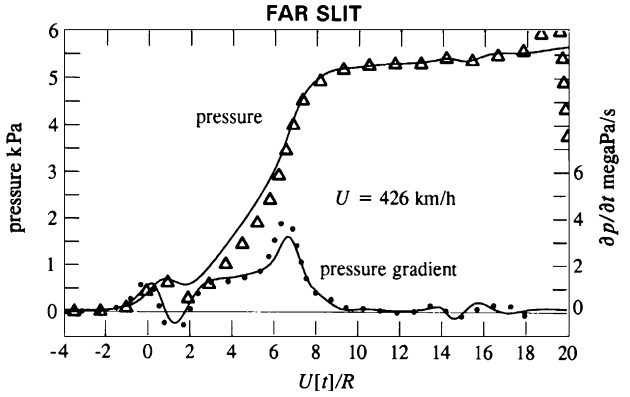

Fig. 17. Measured (△, •) and predicted (——) compression wave pressure and pressure gradient for Case 1 of Fig. 15: $R_h = 1.25R$, $\ell_w = 0.06R$, $z_t = -0.4R$ for the model scale train defined by Eqs. (33), (34) and (42), with $U = 426\,\mathrm{km/h}$ when $\mu = 0.047$. The slit window and its modelling by 10 equal rectangular windows are defined in Eqs. (49) and (50). Measurements are made within the tunnel at a distance of 1.5 m from the hood entrance plane.

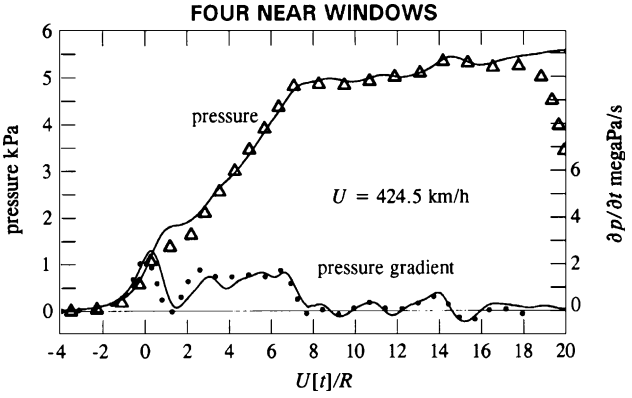

Fig. 18. Measured (△, •) and predicted (——) compression wave pressure and pressure gradient for Case 2 of Fig. 15: $R_h = 1.25R$, $\ell_w = 0.06R$, $z_t = 0.4R$ for the model scale train defined by Eqs. (33), (34) and (42), with $U = 424.5\,\mathrm{km/h}$ when $\mu = 0.047$. The dimensions of the four windows are defined in Eq. (51). Measurements are made within the tunnel at a distance of 1.5 m from the hood entrance plane.

9.2. Case 2

There are four windows for which

$$\left.\begin{aligned} &\ell_x = 0.74R,\ \ell_\theta = 0.4R, \quad \text{at } x_1 = -2R \\ &\ell_x = 0.74R,\ \ell_\theta = 0.4R, \quad \text{at } x_2 = -4R \\ &\ell_x = 0.74R,\ \ell_\theta = 0.4R, \quad \text{at } x_3 = -6R \\ &\ell_x = 0.6R,\ \ell_\theta = 0.4R, \quad \text{at } x_4 = -7.93R \end{aligned}\right\}. \tag{51}$$

Comparisons of predictions and experiment for $U = 424.5\,\mathrm{km/h}$ and $z_t = \pm 0.4R$ are displayed, respectively, in Figs. 18 and 19, in which we have again taken $\mu = 0.047$ to obtain the best overall agreement at later values of $U[t]/R$. The agreement between theory and experiment at this high Mach number is arguably excellent.

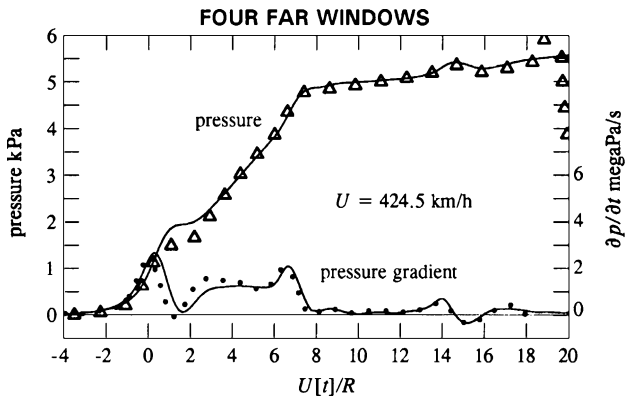

Fig. 19. Measured (△, •) and predicted (——) compression wave pressure and pressure gradient for Case 2 of Fig. 15: $R_h = 1.25R$, $\ell_w = 0.06R$, $z_t = -0.4R$ for the model scale train defined by Eqs. (33), (34) and (42), with $U = 424.5\,\mathrm{km/h}$ when $\mu = 0.047$. The dimensions of the four windows are defined in Eq. (51). Measurements are made within the tunnel at a distance of 1.5 m from the hood entrance plane.

10. Conclusion

An ability to perform rapid numerical predictions of the compression wave generated by a high-speed train entering a vented tunnel portal permits the designer to investigate with minimal delay many possible configurations involving windows of different sizes and distribution, a range of possible hood lengths and diameter, and a selection of different train nose profiles. The method of calculation proposed in this paper considers only the simplest case of circular cylindrical tunnels and hoods of the type employed in model scale testing and design studies. The whole calculation can be executed in much less than a minute on a personal computer. This should be contrasted with the tens or hundreds of hours required for predictions using full Euler or Navier–Stokes simulations on a high performance supercomputer. Our results represent the first step in the development of a general algorithm based on the same approach and applicable to tunnels and hoods of arbitrary cross-sectional dimensions and shape.

The present limited scheme has been validated by comparison with model scale experiments performed at the Railway Technical Research Institute in Tokyo (some of which are reported in Sections 7–9 of this paper) at train Mach numbers as large as $M \sim 0.35$. This exceeds the Mach numbers of the fastest trains currently in regular service. Further comparisons with experiments are needed, however, to check predictions at the highest anticipated operational Mach numbers ~ 0.45 of the next generation of very high-speed trains of the *Maglev* type.

Acknowledgement

The work reported in this paper is sponsored by the Railway Technical Research Institute, Tokyo, Japan.

References

[1] T. Hara, Aerodynamic force acting on a high speed train at tunnel entrance, *Bulletin of the Japan Society of Mechanical Engineers* 4 (1961) 547–553.

[2] T. Hara, M. Kawaguti, G. Fukuchi, A. Yamamoto, Aerodynamics of high-speed train, *Monthly Bulletin of the International Railway Congress Association* XLV (2) (1968) 121–146.

[3] S. Ozawa, Y. Morito, T. Maeda, M. Kinosita, Investigation of the pressure wave radiated from a tunnel exit, Railway Technical Research Institute Report No. 1023, 1976 (in Japanese).

[4] W.A. Woods, C.W. Pope, Secondary aerodynamic effects in rail tunnels during vehicle entry, *Proceedings of the Second BHRA Symposium of the Aerodynamics and Ventilation of Vehicle Tunnels*, Cambridge England, 23–25 March 1976, Paper C5, pp. 71–86.

[5] W. Tollmien, Luftwiderstand und Druckverlauf bei der Fahrt von Zügen in einem Tunnel, *Zeitschrift des Vereines Deutscher Ingenieure* 71 (6) (1927) 199–203.
[6] R.G. Gawthorpe, Aerodynamics of trains in tunnels, *Railway Engineer International* 3 (4) (1978) 41–47.
[7] S. Ozawa, T. Maeda, Tunnel entrance hoods for reduction of micro-pressure wave, *Quarterly Report of the Railway Technical Research Institute* 29 (3) (1988) 134–139.
[8] S. Ozawa, T. Maeda, T. Matsumura, K. Uchida, H. Kajiyama, K. Tanemoto, Countermeasures to reduce micro-pressure waves radiating from exits of Shinkansen tunnels, in: A. Haerter (Ed.), *Aerodynamics and Ventilation of Vehicle Tunnels*, Elsevier Science Publishers, 1991, pp. 253–266.
[9] T. Maeda, T. Matsumura, M. Iida, K. Nakatani, K. Uchida, Effect of shape of train nose on compression wave generated by train entering tunnel, in: M. Iguchi (Ed.), *Proceedings of the International Conference on Speedup Technology for Railway and Maglev Vehicles*, Yokohama, Japan, 22–26 November, 1993, pp. 315–319.
[10] T. Ogawa, K. Fujii, Numerical simulation of compressible flows induced by a train moving into a tunnel, *Computational Fluid Dynamics Journal* 3 (1994) 63–82.
[11] T. Ogawa, K. Fujii, Numerical investigation of three dimensional compressible flows induced by a train moving into a tunnel, *Journal of Computers and Fluids* 26 (1997) 565–585.
[12] M. Iida, T. Matsumura, K. Nakatani, T. Fukuda, T. Maeda, Optimum nose shape for reducing tunnel sonic boom, Institution of Mechanical Engineers Paper, C514/015/96, 1996.
[13] R. Gregoire, J. M. Rety, V. Moriniere, M. Bellenoue, T. Kageyama, Experimental study (scale 1/70th) and numerical simulations of the generation of pressure waves and micro-pressure waves due to high-speed train-tunnel entry, in: J.R. Gillard (Eds.), *Proceedings of the 9th International Conference on Aerodynamics and Ventilation of Vehicle Tunnels*, Aosta Valley, Italy, ME Publications, London, 6-8 October 1997, pp. 877–902.
[14] Y. Noguchi, Y. Okamura, K. Uchida, T. Ishihara, S., Mashimo, M. Kageyama, Solving aerodynamic environmental problems arising from train speed-up, Institution of Mechanical Engineers Paper C514/039/96, 1996.
[15] K. Matsuo, T. Aoki, S. Mashimo, E. Nakatsu, Entry compression wave generated by a high-speed train entering a tunnel, in: J.R. Gillard (Ed.), *Proceedings of the 9th International Conference on Aerodynamics and Ventilation of Vehicle Tunnels*, Aosta Valley, Italy, ME Publications, London, 6-8 October 1997, pp. 925–934.
[16] M. Ito, Improvement to the aerodynamic characteristics of Shinkansen rolling stock, *Proceedings of the Institution of Mechanical Engineers Part F, Journal of Rail and Rapid Transit* 214 (2000) 135–143.
[17] J.L. Peters, Tunnel optimized train nose shape, *Paper presented at the 10th International Symposium on Aerodynamics and Ventilation of Vehicle Tunnels*, Boston, USA, 1–3 November, 2000.
[18] S. Ozawa, T. Uchida, T. Maeda, Reduction of micro-pressure wave radiated from tunnel exit by hood at tunnel entrance, *Quarterly Report of the Railway Technical Research Institute* 19 (2) (1978) 77–83.
[19] S. Ozawa, T. Maeda, Model experiment on reduction of micro-pressure wave radiated from tunnel exit, in: R.I. Emori (Ed.), *Proceedings of the International Symposium on Scale Modeling*, Tokyo, Seikei University, Japan Society of Mechanical Engineers, 18–22 July, 1988, pp. 33–37.
[20] M.S. Howe, M. Iida, T. Fukuda, T. Maeda, Theoretical and experimental investigation of the compression wave generated by a train entering a tunnel with a flared portal, *Journal of Fluid Mechanics* 425 (2000) 111–132.
[21] M.S. Howe, M. Iida, T. Fukuda, Influence of an unvented tunnel entrance hood on the compression wave generated by a high-speed train, *Journal of Fluids and Structures* 17 (2003) 833–853.
[22] M.S. Howe, M. Iida, T. Fukuda, T. Maeda, Aeroacoustics of a tunnel-entrance hood with a rectangular window, *Journal of Fluid Mechanics* 487 (2003) 211–243.
[23] M.S. Howe, M. Iida, Influence of separation on the compression wave generated by a train entering a tunnel, *International Journal of Aeroacoustics* 2 (2003) 13–33.
[24] A.E. Vardy, B. Dayman, Alleviation of tunnel entry pressure transients: 2. Theoretical modelling and experimental correlation, *Paper H3 of the Third International Symposium on the Aerodynamics and Ventilation of Vehicle Tunnels*, Sponsored by BHRA Fluid Engineering; University of Sheffield, 19–21 March, 1979, pp. 363–376.
[25] M.S. Howe, On the role of separation in compression wave generation by a train entering a tunnel hood with a window, *Institute of Mathematics and its Applications, Journal of Applied Mathematics* 70 (2003) 400–418.
[26] B. Auvity, M. Bellenoue, Vortex structure generated by a train-tunnel entry near the portal. Paper presented at the *Eighth International Symposium on Flow Visualization*, Sorrento, Italy, 1–4 September, 1998.
[27] B. Auvity, M. Bellenoue, T. Kageyama, Experimental study of the unsteady aerodynamic field outside a tunnel during train entry, *Experiments in Fluids* 30 (2001) 221–228.
[28] T. Fukuda, M. Iida, M. Suzuki, Visualization of unsteady flow generated by a train entering a tunnel, *Proceedings of Utsunomiya Visualization Symposium*, The Visualization Society of Japan, Utsunomiya, Japan, 31 October–1 November, 2003, pp. 63–66.
[29] M.S. Howe, *Acoustics of Fluid–Structure Interactions*, Cambridge University Press, Cambridge, 1998.
[30] B. Noble, *Methods based on the Wiener-Hopf Technique*, Pergamon Press, London, 1958 (Reprinted 1988 by Chelsea Publishing Company, New York.).
[31] Lord Rayleigh, *The Theory of Sound*, vol. 2, Macmillan, London, 1926.
[32] J. Lighthill, *Waves in Fluids*, Cambridge University Press, Cambridge, 1978.
[33] M.S. Howe, The compression wave produced by a high-speed train entering a tunnel, *Proceedings of the Royal Society A* 454 (1988) 1523–1534.
[34] M.J. Lighthill, *An Introduction to Fourier Analysis and Generalised Functions*, Cambridge University Press, Cambridge, 1958.

[35] A. Cummings, Acoustic nonlinearities and power losses at orifices, *American Institute of Aeronautics and Astronautics Journal* 22 (1984) 786–792.
[36] A. Cummings, Transient and multiple frequency sound transmission through perforated plates at high amplitude, *Journal of the Acoustical Society of America* 79 (1986) 942–951.
[37] M. Iida, Y. Sakuma Unpublished tests performed at the Railway Technical Research Institute, Tokyo, 2002.